Dynamics, transition states, and timing of bond formation in Diels–Alder reactions

Kersey Black[a], Peng Liu[b], Lai Xu[b], Charles Doubleday[c,1], and Kendall N. Houk[b,1]

[a]Keck Science Department, Claremont McKenna, Pitzer and Scripps Colleges, 925 N Mills Avenue, Claremont, CA 91711-5916; [b]Department of Chemistry and Biochemistry, University of California, Los Angeles, CA 90095-1569; and [c]Department of Chemistry, Columbia University, 3000 Broadway, MC 3142, New York, NY 10027

This contribution is part of the special series of Inaugural Articles by members of the National Academy of Sciences elected in 2010. Contributed by Kendall N. Houk, June 7, 2012 (sent for review April 23, 2012)

The time-resolved mechanisms for eight Diels–Alder reactions have been studied by quasiclassical trajectories at 298 K, with energies and derivatives computed by UB3LYP/6-31G(d). Three of these reactions were also simulated at high temperature to compare with experimental results. The reaction trajectories require 50–150 fs on average to transverse the region near the saddle point where bonding changes occur. Even with symmetrical reactants, the trajectories invariably involve unequal bond formation in the transition state. Nevertheless, the time gap between formation of the two new bonds is shorter than a C—C vibrational period. At 298 K, most Diels–Alder reactions are concerted and stereospecific, but at high temperatures (approximately 1,000 K) a small fraction of trajectories lead to diradicals. The simulations illustrate and affirm the bottleneck property of the transition state and the close connection between dynamics and the conventional analysis based on saddle point structure.

molecular dynamics | density functional theory | transition state theory | cycloadditions | concerted reaction

The Diels–Alder reaction is one of the most important reactions used in organic synthesis (1, 2), and its discovery was recognized by the Nobel Prize in Chemistry in 1950. The reaction is a paradigm for methods that efficiently increase structural complexity, because two single bonds, a six-membered ring, and up to four stereocenters are formed in a single step.

Mechanisms of Diels–Alder reactions have been the subject of intensive scrutiny by experimental and theoretical methods (3–6). The timing of bond formation has been the focus of attention. Many experimental studies show that the Diels–Alder reaction is stereospecific with respect to both reactants (7), a result that is compatible with a concerted mechanism, traditionally defined as a reaction path involving no intermediates. DFT and ab initio calculations based on transition state theory predict that a concerted, one-step mechanism is the lowest energy pathway on the ground-state potential energy surface (PES) (8). However, at the time-resolved level, the two new carbon–carbon bonds may not form simultaneously along a dynamical trajectory. The time gap between formation of the two bonds is strongly connected to the expected degree of stereospecificity observed in the reaction, but the details of this relationship are uncertain due to several recent reports: (*i*) In studies of *retro*-Diels–Alder (*retro*-DA) dynamics at femtosecond time resolution of reaction *R2* in Scheme 1, Zewail and coworkers found two sets of transients, one identified with concerted asynchronous trajectories, the other with diradicaloid stepwise trajectories (9, 10). Because reactants are photochemically activated, a full understanding of the experiments must include the role of conical intersections between ground and excited states (11). (*ii*) In thermal shock tube studies of the *retro*-DA reactions *R1*, *R2*, and *R3* in Scheme 1, Lewis, Baldwin, and coworkers found that the *retro*-DA reaction of *cis*-4,5-d_2-cyclohexene (*R1*) at 1,094–1,180 K yields 5–9% *trans*-d_2-ethylene (12), but *retro*-DA reactions of norbornene-d_2 (*R2*) and [2.2.2]bicyclooctene-d_2 (*R3*) showed no measurable loss of stereochemistry (13). They suggest that the stereochemical inversion in *retro-R1* is due to greater conformational flexibility in the region of the cyclohexene ring-opening transition state (TS) than for the bicyclic analogs, such that diradical geometries can be accessed in the *retro-R1* reaction (13). Conversely, diradicals might always be formed but are rarely manifested in experiments, a point of view championed by Firestone (6).

We report quasiclassical trajectory calculations for eight Diels–Alder reactions shown in Scheme 1. *R1–3* were also simulated at high temperature (1,180 K, 849 K, and 1,017 K, respectively). Scheme 1 includes the six symmetric cases of butadiene, cyclopentadiene, and cyclohexadiene reacting with ethylene and acetylene, *R1–6*, and two unsymmetrical reactions, butadiene and 2-hydroxybutadiene reacting with cyanoacetylene, *R7* and *R8*. In *R8*, the hypothetical 2-hydroxybutadiene is a model of the highly reactive Danishefsky diene (14). The calculations give the distribution of forming bond lengths in the transition zone, the time gap between the first and second bond formation, and the effects of temperature and substituents on the transition zone and dynamics. The trajectories at 298 K are concerted and stereospecific, except for the highly asymmetric reaction *R8*, for which 3% of the trajectories form diradicals. At high temperature, 2% of reaction *R1* and 1% of *R3* also give diradicals.

For each reaction in Scheme 1, B3LYP/6-31G(d) was used to locate the saddle point for concerted addition and propagate the trajectories. B3LYP activation barriers are a few kcal/mol higher than the M06-2X/6-31G(d) results (Scheme 1), as a result of the systematic error of B3LYP in treating π vs. σ bonds (15). However, the geometries of transition structures are not sensitive to the choice of density functionals (see *SI Appendix*, Fig. S13). Scheme 1 also shows the energies to distort reactants into transition state geometries (ΔE_{dist}), which is the major component of the activation energy and a quantity that must be overcome by the thermal vibrational excitation of reactants (16–19).

Quasiclassical trajectories were initialized at the concerted saddle points by TS normal mode sampling (20–22), with a customized version of the Venus dynamics program (23). The importance of the TS distribution (coordinates and momenta) in determining the products is well recognized (24, 25). In trajectory calculations of organic reactions, the momentum distribution of the TS has a critical effect on product selectivity, as Carpenter was the first to point out (26–28). In a recent illustration of this effect in a Diels–Alder reaction, Singleton and coworkers found that the product ratio predicted by trajectory calculations is strongly correlated with the direction of momenta at the TS (29).

In our trajectory study of a diradical-mediated fourfold degen-

Author contributions: C.D. and K.N.H. designed research; K.B., P.L., L.X., and C.D. performed research; K.B., P.L., L.X., C.D., and K.N.H. analyzed data; and K.B., P.L., C.D., and K.N.H. wrote the paper.

The authors declare no conflict of interest.

[1]To whom correspondence may be addressed. E-mail: houk@chem.ucla.edu or ced3@columbia.edu.

This article contains supporting information online at www.pnas.org/lookup/suppl/doi:10.1073/pnas.1209316109/-/DCSupplemental.

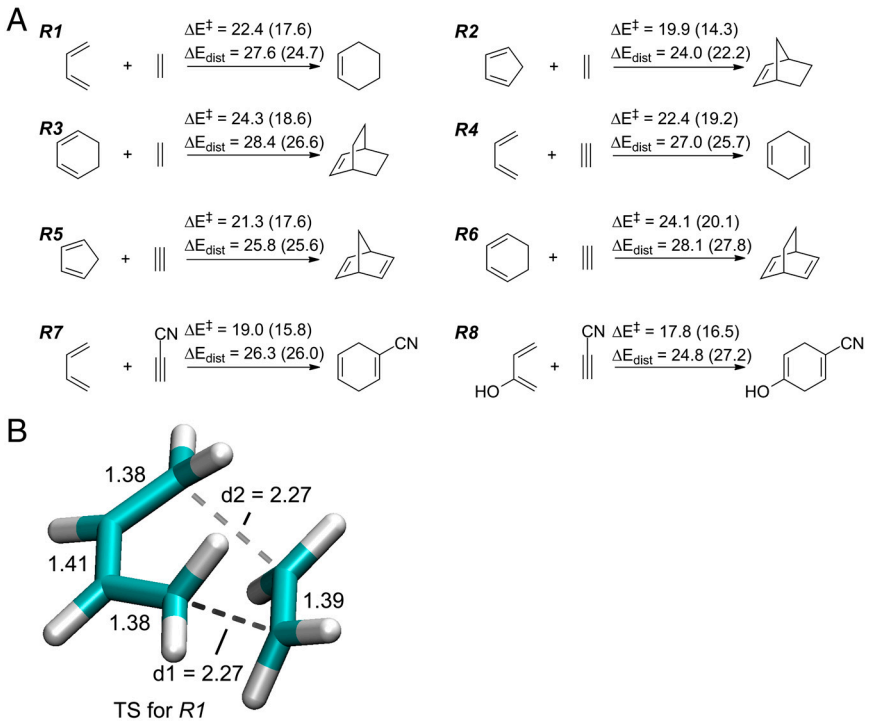

Scheme 1. (*A*) Diels–Alder reactions *R1-R8* investigated by trajectory calculations. B3LYP/6-31G(d) and M06-2X/6-31G(d) (in parentheses) activation barriers and distortion energies of reactants at the saddle point geometries are given in kcal/mol. See *SI Appendix*, Scheme S1, for activation enthalpies and free energies for these reactions. (*B*) Saddle point for reaction *R1* optimized by B3LYP/6-31G(d). Bond distances are given in angstrom. Carbon: cyan; hydrogen: white. See *SI Appendix* for TS geometries for other reactions.

erate rearrangement (30) reported experimentally by Baldwin and Keliher (31), we found that the product ratio is related in a simple way to the momentum distribution at the TS and that the distribution of structures is also important. A closely related issue is post-TS product selectivity, often on a bifurcating PES (32, 33) or involving chemical activation of an intermediate from high energy reactants (34, 35). The sampling procedure in the present study uses harmonic frequencies and normal modes at the TS to generate a set of coordinates and momenta that approximate a quantum mechanical Boltzmann distribution of vibrational levels on the TS dividing surface. At 298 K, trajectories were initialized at the lowest energy saddle point for each reaction in Scheme 1. High temperature trajectories were initialized at variational transition states for concerted cycloaddition located by Polyrate (36) at 1,180 K for *R1*, 849 K for *R2*, and 1,017 K for *R3*. For each reaction, 128 or 256 trajectories were computed.

Starting from these sampled coordinates and momenta, trajectories were propagated in both forward and reverse directions until either the cycloadduct is formed (both forming C—C bond lengths <1.6 Å) or reactants are separated by >5 Å. The classical equations of motion are integrated with a Hessian-based predictor-corrector algorithm (37) using Gaussian 09 (38) with energies and derivatives computed "on the fly" by UB3LYP/6-31G(d). Step lengths of 0.12 amu$^{1/2}$·Bohr (approximately 0.3 fs per step) for reactions *R1–6* and 0.25 amu$^{1/2}$·Bohr (approximately 0.7 fs per step) for reactions *R7* and *R8* were used, and the force constants were updated every 12 steps. This gives very similar propagation results to trajectories propagated with a step length of 0.10 amu$^{1/2}$·Bohr (approximately 0.25 fs) and update of force constants every two steps (see *SI Appendix*). Trajectories are reactive if cycloadduct is formed in one direction and reactants in the other. The forward and reverse trajectory simulations from the same initial geometry give the complete trajectory that connects reactants, transition state, and product. About 10% of trajectories recross the TS to form the same species in the forward and reverse directions. These are ignored.

Although the saddle points for reactions *R1–6* are symmetrical and the two forming C—C bond lengths are identical (4, 5), the distribution of sampled TS geometries contains many asynchronous structures. Fig. 1 shows the overlay of sampled TS geometries and the corresponding C—C bond length distributions. The average asynchronicities of the initial geometries, defined as the average difference in length of the two forming carbon–carbon bonds, are summarized in Table 1. The average asynchronicity consists of static asynchronicity of the saddle point and the dynamic asynchronicity contributed by TS normal mode sampling. For symmetrical reactions (*R1–6*), the asynchronicities are entirely induced by dynamics. At high temperature, the distribution of C—C bond lengths at the concerted TS broadens considerably. The average asynchronicities for *R1–6* are approximately 0.2 Å at 298 K and up to 0.3 Å at 849–1,180 K. For the unsymmetrical reactions *R7* and *R8*, contributions from both static and dynamic asynchronicity lead to a much more asynchronous TS distribution. Due to the structural asynchronicities of forming C—C bond lengths, the two bonds are not formed simultaneously in these dynamical trajectories. The time gap of bond formation will be discussed later.

The distribution of forming C—C bond lengths in the sampled TS geometries is shown in Fig. 1. The C—C bond lengths are distributed symmetrically with respect to the bond lengths at the saddle point (marked with a red line). To discuss these distributions, we define the "transition zone" as the subset of sampled C—C bonds at the TS such that the deviations in C—C bond length from the bond length at the saddle point is below the 98th percentile. For example, in reaction *R1* at 298 K, 98% of the forming C—C bond lengths in the TS geometries are within ±0.25 Å of the C—C bond length at the saddle point (2.27 Å); the transition zone for reaction *R1* is 2.27 ± 0.25 Å (Formally, the transition state is a hypersurface in phase space (coordinates and momenta). We define the transition zone as a subset the configuration-space part of TS phase space. We also note that the transition zone is computed in the harmonic approximation, and is subject to the usual inaccuracies associated with low frequencies.). Table 1 lists the transition zones for all reactions investigated. For unsymmetrical reactions (*R7–8*), the transition zone of the two forming C—C bonds is calculated for each bond. The widths of the transition zones of the shorter forming C—C bond are similar to those in the symmetrical reactions (about ±0.2 ~ 0.3 Å). The transition zone of the longer forming C—C bond in these unsymmetrical reactions is wider (up to ±0.5 Å).

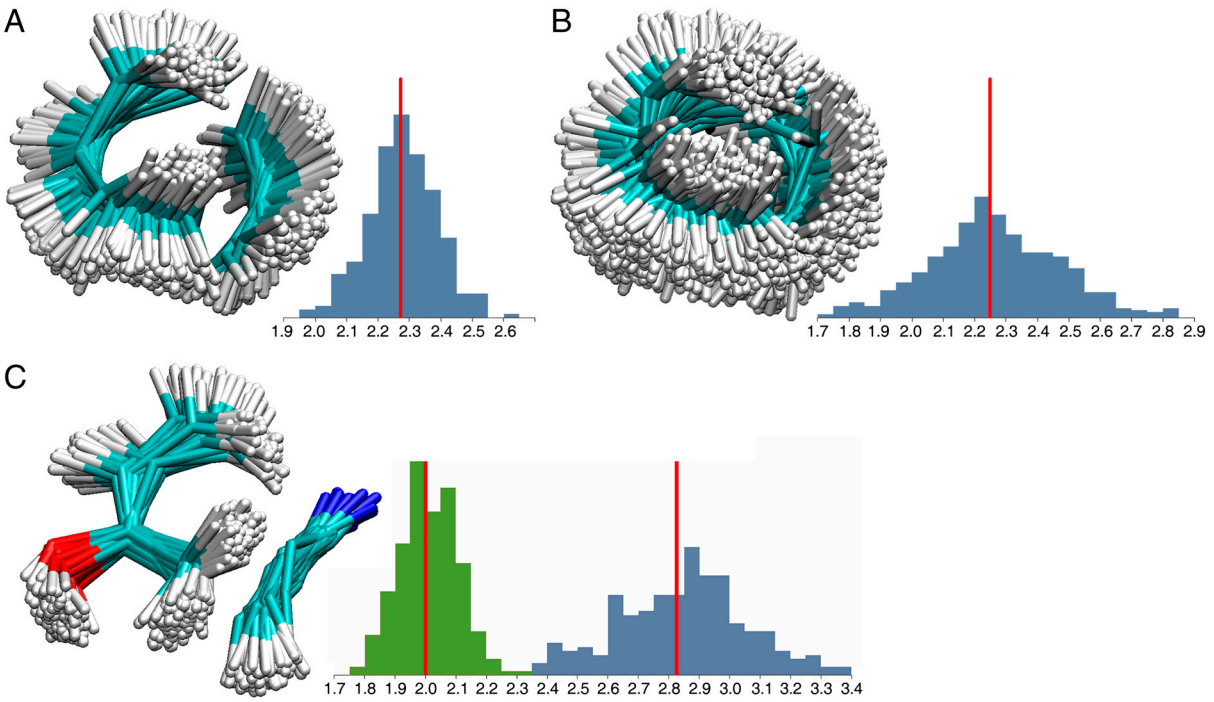

Fig. 1. Superposition of sampled TS geometries in the reactions of (*A*) butadiene and ethylene at 298 K (*R1*, Scheme 1); (*B*) butadiene and ethylene at 1,180 K; (*C*) 2-hydroxybutadiene and cyanoacetylene at 298 K (*R8*, Scheme 1). The distribution of forming C—C bond lengths in TS geometries are shown. The forming C—C bond length at the saddle point is marked with a red line in each of the distribution plots. See *SI Appendix* for similar figures for other reactions.

Plots of the two forming C—C bond distances for reactive trajectories in several reactions are shown in Fig. 2 along with plots of C—C bond distance vs. time. The sampled TS points (initial trajectory points) for each trajectory are marked with blue dots in the distance versus distance plots (Fig. 2 *A–C*). This set of points is the 2D projection of the transition state coordinate distribution, located on the TS dividing surface orthogonal to the minimum energy reaction path. At 298 K, the trajectories are similar for all six symmetric Diels–Alder reactions (Fig. 2*A* and *SI Appendix*, Fig. S3), and all trajectories in these reactions lead directly to the product. Most C—C bonds in reactions *R1–6* are formed within 50 fs after crossing the TS (Fig. 2*D* and *SI Appendix*, Fig. S5). The very short time of bond formation leads to even shorter time gap between the formation of the two C—C bonds, less than 5 fs on average for reactions *R1–6* (Table 2; see Movie S1 for a typical trajectory of *R1* at 298 K). These time gaps are all much shorter than the lifetimes of C—C bond stretching vibrations (*ca.* 30–60 fs), so that we describe these Diels–Alder reactions as dynamically concerted (39).

Table 1. Average asynchronicity of transition state geometry and definition of transition zone

Reaction	T (K)	C—C distance at saddle point (Å)	Average asynchronicity of the TS geometry (Å)	Transition zone (Å) *	No. of reactive and total trajectories
R1	298	2.27	0.17 ± 0.13	2.27 ± 0.25	117/128
	1,180	2.25	0.32 ± 0.26	2.25 ± 0.46	226/256
R2	298	2.25	0.16 ± 0.10	2.25 ± 0.22	124/128
	849	2.23	0.27 ± 0.20	2.23 ± 0.38	237/256
R3	298	2.28	0.16 ± 0.12	2.28 ± 0.23	112/128
	1,017	2.25	0.25 ± 0.24	2.25 ± 0.42	204/256
R4	298	2.30	0.20 ± 0.13	2.30 ± 0.25	117/128
R5	298	2.27	0.21 ± 0.14	2.27 ± 0.27	123/128
R6	298	2.29	0.18 ± 0.14	2.29 ± 0.29	112/128
R7	298	2.10	0.50 ± 0.26	2.10 ± 0.24	225/256
		2.61		2.61 ± 0.38	
R8	298	2.00	0.83 ± 0.30	2.00 ± 0.21	211/256
		2.83		2.83 ± 0.46	

*Transition zone is defined as a region that includes 98% of the initial transition state geometries.

At 1,180 K, most trajectories for reaction *R1* still lead directly to product, although the TS distribution has broadened to include more asynchronous structures (Movie S2). As shown in Fig. 2*B*, the wider distribution of TS asynchronicity and increased thermal energy have enabled 1.8% of the trajectories to traverse through the region in which one bond is formed (<1.6 Å) while the other bond is yet to be formed (>2.6 Å). This region corresponds to intermediates with strong diradical character ($S^2 \approx 1$ in UDFT). These diradical intermediates have lifetimes of 800–1,500 fs, long enough for rotation about the ethylene C—C bond to be observed (Movie S3). There will be loss of stereospecificity in these trajectories with labeled reactants (5, 8). Similarly, 1.0% of trajectories in the reaction of cyclohexadiene and ethylene (*R3*) lead to diradicals at 1,017 K, while no trajectories in the reaction of cyclopentadiene and ethylene (*R2*) at 849 K involve diradical intermediates. Lewis and Baldwin determined that the *retro*-DA reaction of *cis*-4,5-d_2-cyclohexene (*R1*) at 1,180 K yields 9% *trans*-d_2-ethylene (12), and the maximum amount of *trans*-d_2-ethylene that could have gone undetected was 1.3% for *R2* and 6.3% for *R3* (13). We have not included an estimate of diradicals formed from the higher energy stepwise TS.

The reactions of butadiene and 2-hydroxybutadiene with cyanoacetylene (Fig. 2*C* and *SI Appendix*, Fig. S3) are much more asynchronous than are the symmetric reactions. At 298 K, most trajectories are still dynamically concerted, leading to the products without formation of intermediates (Movie S4). The average time gaps for bond formation in reactions *R7* and *R8* are 15 and 57 fs, respectively, much greater than those of the symmetrical Diels–Alder reactions. For *R7*, 99% of the trajectories have time gaps less than 100 fs, and 1% are in the range 100–200 fs. For *R8*, 89% have time gaps less than 100 fs, and 97% are less than 200 fs. The time gaps in these extremely asynchronous Diels–Alder reactions are within the lifetime of several C—C stretching vibrations. All trajectories in the reaction of cyanoacetylene and

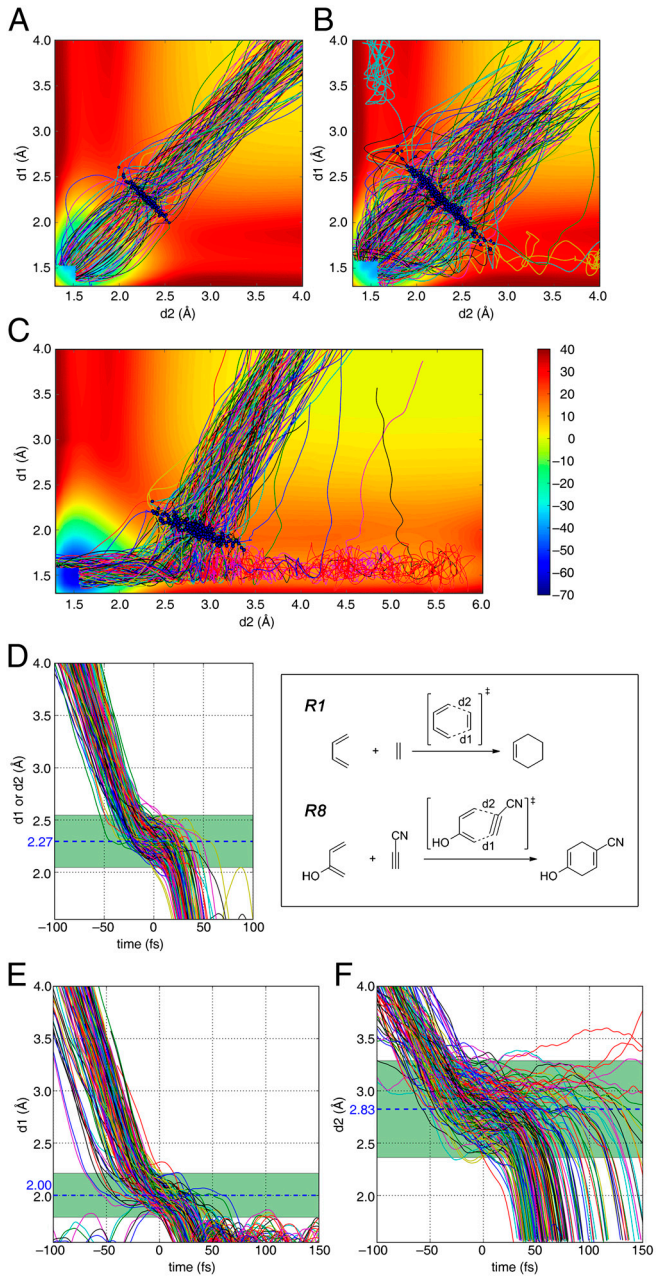

Fig. 2. (*A–C*) Distances of the two forming C—C bonds in reactions *R1* at 298 K, *R1* at 1,180 K, and *R8* at 298 K, respectively. Contour plots are calculated with UB3LYP/6-31G(d). Energies are in kcal/mol relative to separate reactants. (*D*) forming C—C bond lengths vs. time in *R1* at 298 K. (*E* and *F*) Shorter bond (d1) and longer bond (d2) lengths vs. time in *R8* at 298 K. Time zero is the time at which the trajectory crosses the TS—i.e., the starting point of each trajectory. Trajectories are stopped when the C—C bond is <1.6 Å. Transition zone is highlighted in green. See *SI Appendix* for plots for other reactions.

butadiene and most of the trajectories in the reaction of cyanoacetylene and 2-hydroxybutadiene are still dynamically concerted.

In the highly asynchronous reaction of 2-hydroxybutadiene with cyanoacetylene (Fig. 2*C*), a few trajectories traverse through the region of diradical intermediates (d1 ≈ 1.6 Å, d2 > 2.7 Å. Movie S5). These intermediates have a lifetime of about 1,000 fs, similar to the diradical intermediates in high-temperature DA reaction *R1* (Reactions like *R7* and *R8* are generally studied in solution, and solvation of such highly polar intermediates should be important in increasing the lifetimes of intermediates. This will be investigated in the future.).

Table 2. Calculated time gaps of bond formation and time in transition zone for Diels–Alder reactions at 298 K

Reaction	Average time gap of C—C bond formation (fs) *	Time to traverse the transition zone (fs) †
R1	3.9 (3.4) ± 2.9	52.6 (50.9) ± 12.0
R2	3.8 (2.9) ± 2.9	55.7 (52.2) ± 19.6
R3	3.1 (2.4) ± 2.7	53.9 (51.0) ± 15.2
R4	4.2 (3.8) ± 3.0	55.0 (52.1) ± 15.0
R5	4.7 (4.1) ± 3.8	58.5 (55.5) ± 16.3
R6	4.0 (3.3) ± 3.8	58.7 (55.3) ± 14.4
R7	15.3 (11.8) ± 16.9	76.8 (74.1) ± 23.6
R8	56.5 (24.8) ± 155.2	134.1 (94.8) ± 204.96

*Time gap between the two forming C—C bonds decreasing to 1.6 Å. Median time gaps are given in parentheses.

†Time between the first bond enters the transition zone and both bonds leave the zone. See Table 1 for definition of transition zone. Median times are given in parentheses.

The concerted/stepwise dichotomy in Diels–Alder reactions has an interesting analog in the recently discovered roaming mechanism for decomposition of formaldehyde and acetaldehyde (40–42). In both cases, trajectories may "stray" from the concerted pathway to give nearly dissociated radical pairs (or diradicals). These may "roam" across the potential energy surface before forming nonradical products. In the Diels–Alder reactions with highly asynchronous saddle point geometries (e.g., *R8*) or for reactions with symmetric saddle points at ≥1,000 K, stepwise trajectories can be derived from the concerted transition state.

Fig. 2 *D–F* gives a time-resolved view of the bond formation process. The transition zones are highlighted in green, and the saddle point bond lengths are shown as dotted lines. In the transition zone, the velocity of bond formation (slope) decreases dramatically as kinetic energy is converted to potential energy. The median time to traverse the transition zone are around 50–55 fs for the six symmetrical reactions (*R1–6*) and up to 100 fs for unsymmetrical reactions (Table 2). After passing through the transition zone, potential energy is converted back to kinetic energy and the C—C bond formation is accelerated.

Fig. 3 shows the passage through the transition zone of reactions *R1* (*A*, *D*) and *R8* (*B*, *C*, *E*, *F*) from another perspective by explicitly plotting the relative velocities of approach of the forming bonds (*A–C*) and the median kinetic and potential energy (*D–F*) as a function of bond length. Fig. 3 *A–F* illustrates and affirms an important feature of transition state theory: that the TS is the region of minimum flux of forward-moving trajectories—the dynamical bottleneck. Because the symmetric C—C stretching mode dominates the transition vector for Diels–Alder reactions, the velocity of bond formation and the kinetic energy are good proxies for the flux along the reaction coordinate. The velocities shown in Fig. 3 *A–C* are actually the major part of the flux because they show the component along the bond axes. The sharp dip in kinetic energy in Fig. 3 *D–F* is dominated by reaction path motion. This is an approximate description because it ignores reaction path curvature due to coupling with transverse modes. Nevertheless, the minima in velocity and kinetic energy clearly illustrate the bottleneck property of the transition state.

A striking feature of Fig. 3 is that these minima all occur at or near the bond length at the saddle point. This provides a clear, dynamically based justification for the importance of the saddle point structure in the analysis of rates of Diels–Alder reactions. It illustrates the close connection of the dynamics with the conventional TS analysis based on saddle point structure: The structure-based analysis is well justified when the dynamical bottleneck is well defined. Fig. 3 *A–C* includes a few trajectories in which the velocity turns momentarily negative, which means the C—C bond length is increasing. This motion is associated with asynchonous trajectories with some vibration of d2 when d1 has essentially reached a bonding distance. Only with the wider, less restrictive,

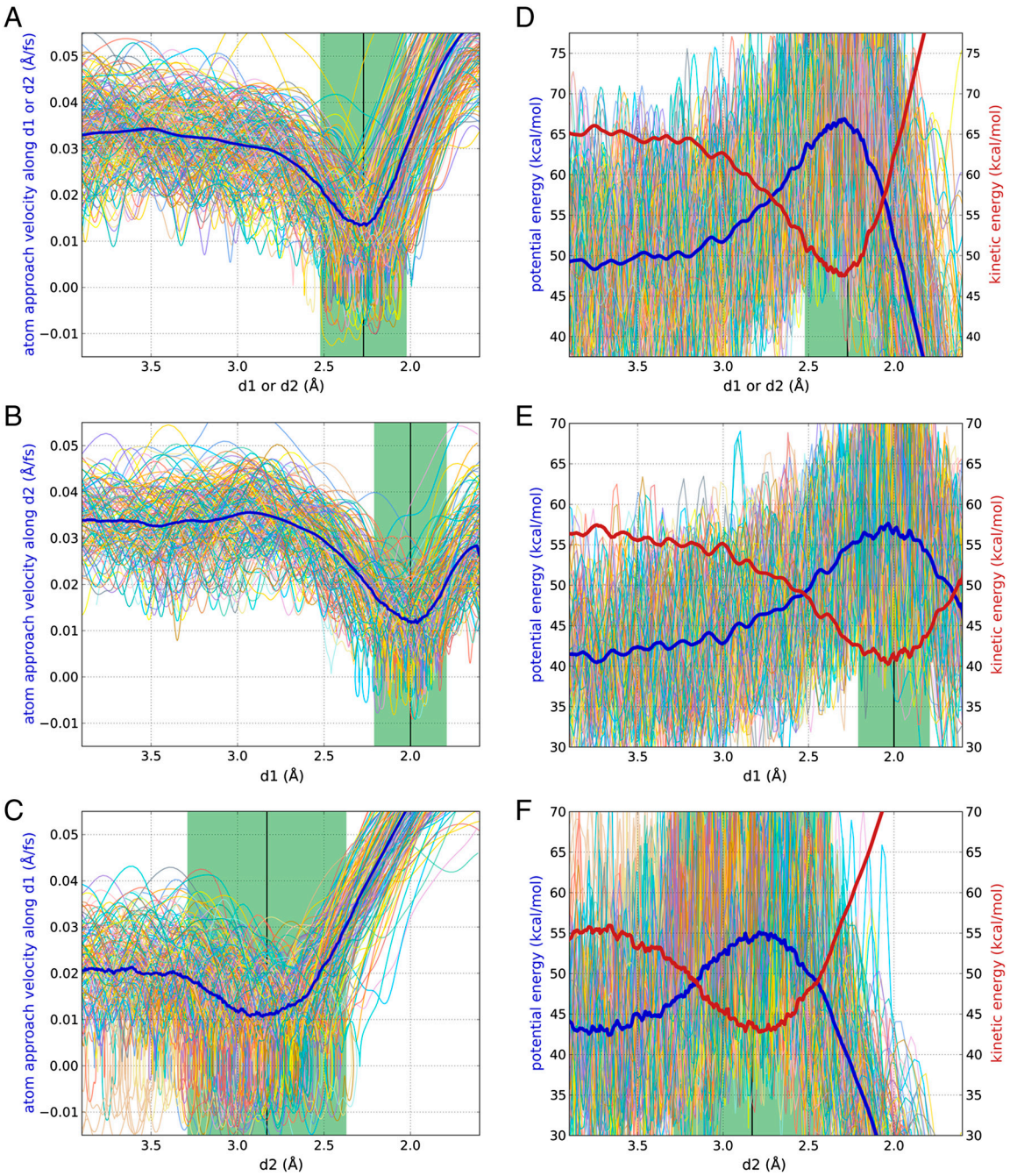

Fig. 3. (*A*) Velocity of C—C bond formation (relative velocity along the bond axis) vs. bond length in *R1*. (*B* and *C*) Velocity of C—C bond formation vs. bond length for the shorter bond (*B*) and longer bond (*C*) in *R8*. In each plot the thin lines represent velocities for individual trajectories, while the median velocity is shown in bold blue. (*D*) Potential energy relative to the electronic energy of separated reactants vs. forming C—C bond length in *R1*. Median kinetic energy (red) and potential energy (blue) are shown in bold. (*E* and *F*) Potential energy vs. forming C—C bond length for the shorter bond (*E*) and longer bond (*F*) in *R8*. Transition zone is highlighted in green. See *SI Appendix* for plots of other reactions.

bottleneck of Fig. 3*C* does this motion lead to 2% diradicals at 298 K.

In summary, the trajectories for the symmetrical Diels–Alder reactions of butadiene, cyclopentadiene, and cyclohexadiene with ethylene or acetylene (*R1–6*) are dynamically concerted, with average time gaps of 5 fs or less, and times to traverse the transition zones averaging 60 fs or less, essentially the lifetime predicted by the preexponential factor of transition state theory. Even the unsymmetrical reaction of butadiene and cyanoacetylene is dynamically concerted—i.e., both C—C bonds are formed within 150 fs for all trajectories at 298 K. For the most asynchronous case, 2-hydroxybutadiene plus cyanoacetylene, 97% of trajectories are still dynamically concerted, but 3% give diradical intermediates at 298 K, even though the trajectories are initialized at the concerted TS. The average time gap of formation of the two C—C bonds is about 5 fs for symmetric Diels–Alder reactions and less than 60 fs for unsymmetric reactions; these time gaps are all shorter than a C—C bond vibrational period. For butadiene plus ethylene at approximately 1,000 K, 2% of trajectories form diradicals. Finally, the simulations illustrate and affirm the bottleneck property of the transition state and the close connection between dynamics

and the conventional transition state analysis based on saddle point structure.

Materials and Methods

Gas phase stationary points (minima and saddle points) were optimized with B3LYP/6-31G(d) using Gaussian 09 (G09) (38). Trajectories were initialized at the saddle points using VMG, Doubleday's customized version of the Venus 96 dynamics package (23). In the VMG option used here, initial coordinates and momenta were chosen by TS normal mode sampling (20–22) with zero-point vibrational energy and vibrational and rotational contributions at 298 K. G09 jobs with the sampled initial conditions were automatically generated to propagate the trajectories (BOMD keyword with ReadVelocity option).

The sampling procedure uses harmonic frequencies and normal modes of the saddle point to generate a set of coordinates and momenta that approximate a quantum mechanical Boltzmann distribution of vibrational levels on the TS dividing surface. Trajectories were run for reactions *R1–8* at 298 K and reactions *R1–3* at higher temperatures: 1,180 K for *R1*, 849 K for *R2*, and 1,017 K for *R3*, which correspond to Lewis and Baldwin's experimental temperatures (12, 13). High temperature trajectories were initialized at variational transition states for concerted cycloaddition located by Polyrate (36). For reactions *R1–6* at 298 K, 128 trajectories were computed. For reactions *R7–8* at 298 K and reactions *R1–3* at high temperatures, 256 trajectories were computed.

Trajectories were propagated in both forward and reverse directions from the initial TS point—i.e., with the same initial coordinates and opposite sign of velocities. The classical equations of motion are integrated with energies and derivatives computed "on the fly" by UB3LYP/6-31G(d). For reactions *R1–6* at 298 K, step lengths of 0.12 amu½·Bohr (approximately 0.3 fs per step) were used. For reactions *R7–8* at 298 K and reactions *R1–3* at high temperatures, step lengths of 0.25 amu½·Bohr (approximately 0.7 fs per step) were used. The force constants were updated every 12 steps. Trajectories were propagated until either the cycloadduct is formed (both forming C—C bond lengths <1.6 Å) or reactants are separated by >5 Å.

ACKNOWLEDGMENTS. We thank the National Science Foundation (NSF) (CHE-1059084 to K.N.H. and CHE-0910876 to C.D.) for financial support of this research. Calculations were performed on the NSF XSEDE resources provided by the XSEDE Science Gateways program (grant TG-CHE090070 to C.D. and TG-CHE040013N to K.N.H.) and on equipment provided by a grant from the John Stauffer Charitable Trust to the Keck Science Department of Claremont McKenna, Pitzer and Scripps Colleges.

1. Diels O, Alder K (1928) Synthesen in der hydroaromatischen reihe (Syntheses in the hydroaromatic series). *Justus Liebigs Ann Chem* 460:98–122.
2. Nicolaou KC, Snyder SA, Montagnon T, Vassilikogiannakis G (2002) The Diels–Alder reaction in total synthesis. *Angew Chem Int Ed* 41:1668–1698.
3. Sauer J, Sustmann R (1980) Mechanistic aspects of Diels–Alder reactions: A critical survey. *Angew Chem Int Ed Engl* 19:779–807.
4. Houk KN, Li Y, Evanseck JD (1992) Transition structures of hydrocarbon pericyclic reactions. *Angew Chem Int Ed Engl* 31:682–708.
5. Houk KN, Gonzalez J, Li Y (1995) Pericyclic reaction transition states: Passions and punctilios, 1935–1995. *Acc Chem Res* 28:81–90 for a contrary view.
6. Firestone RA (1977) The diradical mechanism for 1,3-dipolar cycloadditions and related thermal pericyclic reactions. *Tetrahedron* 33:3009–3039.
7. Houk KN, Lin YT, Brown FK (1986) Evidence for the concerted mechanism of the Diels–Alder reaction of butadiene with ethylene. *J Am Chem Soc* 108:554–556.
8. Beno BR, Wilsey S, Houk KN (1999) The C_7H_{10} potential energy landscape: Concerted transition states and diradical intermediates for the retro-Diels–Alder reaction and [1,3] sigmatropic shifts of norbornene. *J Am Chem Soc* 121:4816–4826.
9. Horn BA, Herek JL, Zewail AH (1996) Retro-Diels–Alder femtosecond reaction dynamics. *J Am Chem Soc* 118:8755–8756.
10. Diau EWG, De Feyter S, Zewail AH (1999) Femtosecond dynamics of retro Diels–Alder reactions: The concept of concertedness. *Chem Phys Lett* 304:134–144.
11. Wilsey S, Houk KN, Zewail AH (1999) Ground- and excited-state reactions of norbornene and isomers: A CASSCF study and comparison with femtosecond experiments. *J Am Chem Soc* 121:5772–5786.
12. Lewis DK, et al. (1993) Concerted and nonconcerted pathways for thermal-conversions of deuterium-labeled cyclohexenes to butadienes and ethylenes. *J Am Chem Soc* 115:11728–11734.
13. Lewis DK, et al. (2001) Stereochemistry of the thermal retro-Diels–Alder reactions of cis,exo-5,6-d_2-bicyclo[2.2.1]hept-2-ene, cis-4,5-d_2-cyclohexene, and cis,exo-5,6-d_2-bicyclo[2.2.2]oct-2-ene. *J Am Chem Soc* 123:996–997.
14. Danishefsky S (1981) Siloxy dienes in total synthesis. *Acc Chem Res* 14:400–406.
15. Pieniazek SN, Clemente FR, Houk KN (2008) Sources of error in DFT computations of C—C bond formation thermochemistries: $\pi \rightarrow \sigma$ transformations and error cancellation by DFT methods. *Angew Chem Int Ed* 47:7746–7749.
16. Ess DH, Houk KN (2007) Distortion/interaction energy control of 1,3-dipolar cycloaddition reactivity. *J Am Chem Soc* 129:10646–10647.
17. Hayden AE, Houk KN (2009) Transition state distortion energies correlate with activation energies of 1,4-dihydrogenations and Diels–Alder cycloadditions of aromatic molecules. *J Am Chem Soc* 131:4084–4089.
18. Xu L, Doubleday CE, Houk KN (2009) Dynamics of 1,3-dipolar cycloaddition reactions of diazonium betaines to acetylene and ethylene: Bending vibrations facilitate reaction. *Angew Chem Int Ed* 48:2746–2748.
19. Xu L, Doubleday CE, Houk KN (2010) Dynamics of 1,3-dipolar cycloadditions: Energy partitioning of reactants and quantitation of synchronicity. *J Am Chem Soc* 132:3029–3037.
20. Chapman S, Bunker DL (1975) Exploratory study of reactant vibrational effects in $CH_3 + H_2$ and its isotopic variants. *J Chem Phys* 62:2890–2899.
21. Doubleday CE, Bolton K, Hase WL (1998) Direct dynamics quasiclassical trajectory study of the thermal stereomutations of cyclopropane. *J Phys Chem A* 102:3648–3658.
22. Peslherbe GH, Wang HB, Hase WL (1999) *Monte Carlo Methods in Chemical Physics*, eds DM Ferguson, JI Siepmann, and DG Truhlar (Wiley, New York), pp 171–201.
23. Hase WL, et al. (1996) *VENUS 96. QCPE* 1996:671.
24. Polanyi JC (1987) Some concepts in reaction dynamics (Nobel lecture). *Angew Chem Int Ed Engl* 26:952–971.
25. Zewail AH (2000) Femtochemistry: Atomic-scale dynamics of the chemical bond using ultrafast lasers (Nobel lecture). *Angew Chem Int Ed* 39:2587–2631.
26. Carpenter BK (1985) Trajectories through an intermediate at a fourfold branch point. Implications for the stereochemistry of biradical reactions. *J Am Chem Soc* 107:5730–5732.
27. Carpenter BK (1995) Dynamic matching: The cause of inversion of configuration in the [1,3] sigmatropic migration? *J Am Chem Soc* 117:6336–6344.
28. Carpenter BK (1998) Dynamic behavior of organic reactive intermediates. *Angew Chem Int Ed* 37:3340–3350.
29. Wang ZH, Hirschi JS, Singleton DA (2009) Recrossing and dynamic matching effects on selectivity in a Diels–Alder reaction. *Angew Chem Int Ed* 48:9156–9159.
30. Doubleday CE, Suhrada CP, Houk KN (2006) Dynamics of the degenerate rearrangement of bicyclo[3.1.0]hex-2-ene. *J Am Chem Soc* 128:90–94.
31. Baldwin JE, Keliher EJ (2002) Activation parameters for three reactions interconverting isomeric 4- and 6-deuteriobicyclo[3.1.0]hex-2-enes. *J Am Chem Soc* 124:380–381.
32. Singleton DA, Hang C, Szymanski MJ, Greenwald EE (2003) A new form of kinetic isotope effect. dynamic effects on isotopic selectivity and regioselectivity. *J Am Chem Soc* 125:1176–1177.
33. Thomas JB, Waas JR, Harmata M, Singleton DA (2008) Control elements in dynamically determined selectivity on a bifurcating surface. *J Am Chem Soc* 130:14544–14555.
34. Vayner G, Addepalli SV, Song K, Hase WL (2006) Post-transition state dynamics for propene ozonolysis: Intramolecular and unimolecular dynamics of molozonide. *J Chem Phys* 125:014317.
35. Lourderaj U, Park K, Hase WL (2008) Classical trajectory simulations of post-transition state dynamics. *Int Rev Phys Chem* 2:361–403.
36. Truhlar DG, et al. POLYRATE 2010-A., http://comp.chem.umn.edu/polyrate.
37. Millam JM, Bakken V, Chen W, Hase WL, Schlegel HB (1999) Ab initio classical trajectories on the Born–Oppenheimer surface: Hessian-based integrators using fifth-order polynomial and rational function fits. *J Chem Phys* 111:3800–3805.
38. Frisch MJ, et al. (2010) *Gaussian 09, Revision B 01* (Gaussian, Inc, Wallingford, CT).
39. Levine RD (2005) *Molecular Reaction Dynamics* (Cambridge Univ Press, Cambridge), pp 184–187.
40. Townsend D, et al. (2004) The roaming atom: Straying from the reaction path in formaldehyde decomposition. *Science* 306:1158–1161.
41. Bowman JM, Shepler BC (2011) Roaming radicals. *Annu Rev Phys Chem* 62:531–553.
42. Harding LB, Klippenstein SJ, Jasper AW (2007) Ab initio methods for reactive potential surfaces. *Phys Chem Chem Phys* 9:4055–4070.